Chapter 9

Modeling Results for Glacier Bay

Finally, attention is now turned to a number of specific results of interest for the Glacier Bay domain.

9.1 Water Surface Elevation

In the previous chapter, some preliminary results on water surface elevation were shown in order to 'validate' the model output. This was done by comparing model output to NOAA predictions and observations at a single station. There are a number of ways that we can now look at the spatial variation of the tides, in terms of magnitude and timing.

9.1.1 Tidal Amplification and Phase Lag

By requesting time series output at a number of stations, the amplification or attenuation of the tidal wave as it propagates up-fjord is readily studied. As shown in Fig. 9.1, time series output was requested at five stations dispersed throughout the domain.

Figure 9.2 shows the model output at these five stations. First, it is clear that the tidal wave amplifies as it propagates up-fjord. This is primarily due to the narrowing of the fjord which produces a shoaling effect on the wave. Second, the 'phase lag' between stations is clearly evident. Station 2 roughly corresponds to Bartlett Cove, station 3 to Willoughby Island, and stations

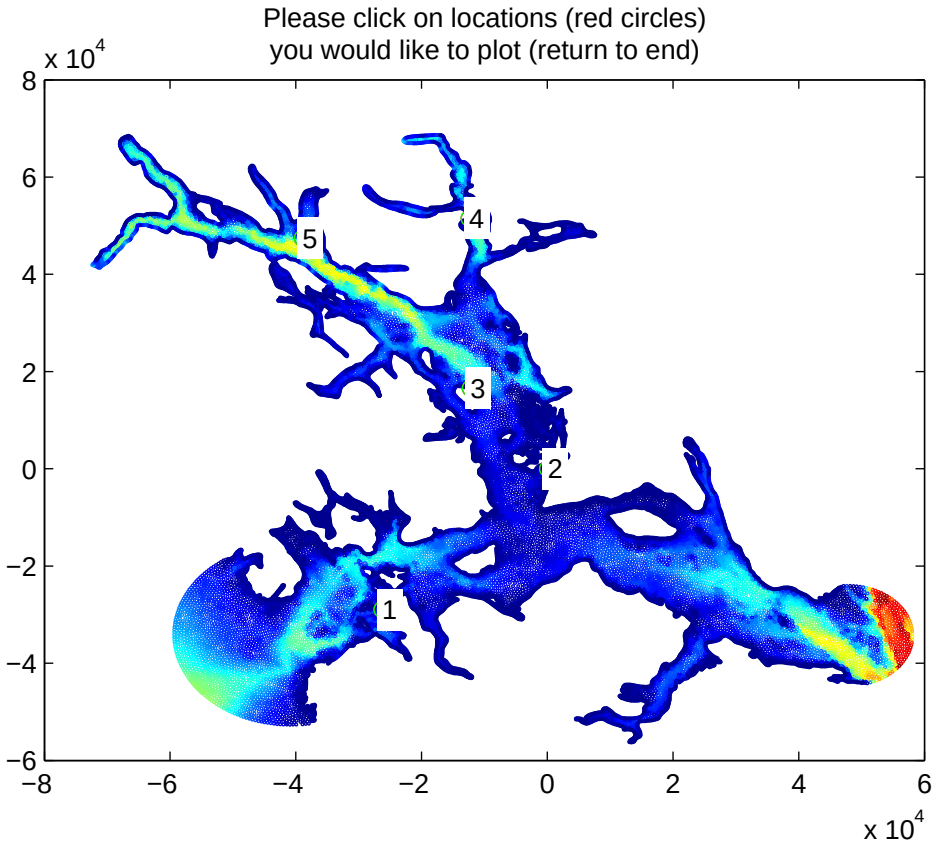

Figure 9.1: Domain map indicating five stations specified for time series output.

5 and 4 to the middle of the East and West Arms respectively. The results indicate a phase lag of approximately 15 to 20 minutes between stations 2 and 3. From station 3 to stations 4 and 5, the lag is only a few minutes. These results are consistent to the corrections published by NOAA.

Additional insight is gained by considering the contours of water surface elevation over the entire domain. Figure 9.3 shows a snapshot of the water surface at the commencement of an ebb tide during spring tide conditions. The tides are relatively low out in the Gulf, somewhat higher in Icy Strait and Cross sound, and higher still in Glacier Bay proper. Within the Bay proper, the variation in tidal amplitude becomes fairly weak.

If the limits on the color contours are changed and a zoomed in view

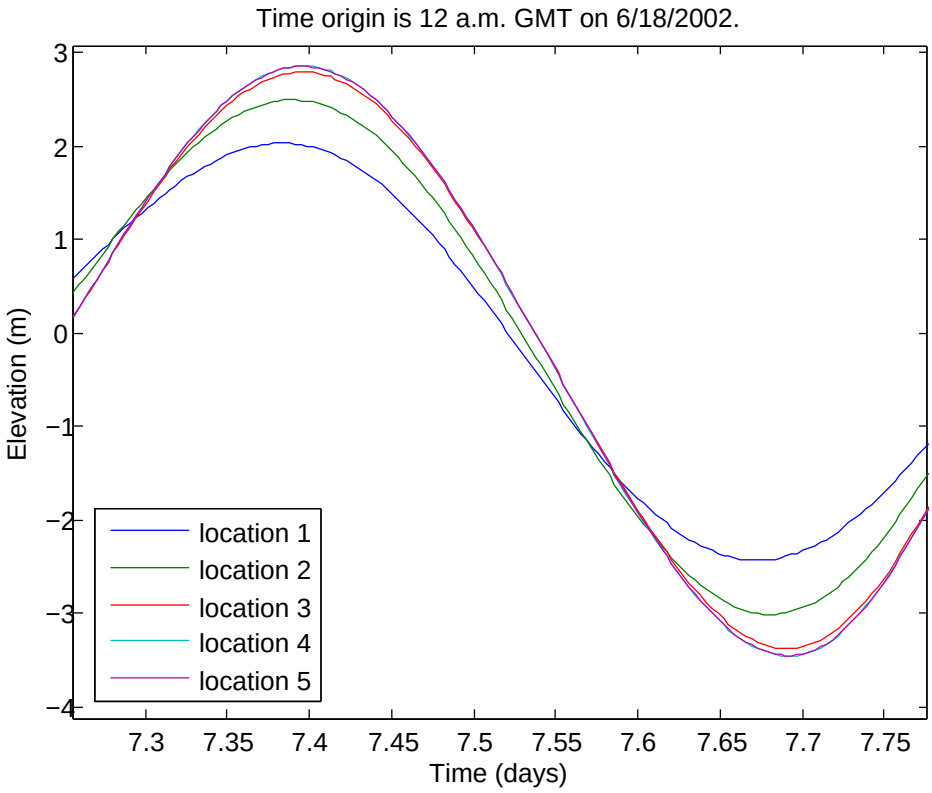

Figure 9.2: Domain map indicating five stations specified for time series output.

is taken (Fig. 9.4), the variation in tidal amplitude with up-fjord distance becomes more apparent. It is found that the highest tides in the bay occur in Adams Inlet in the East Arm.

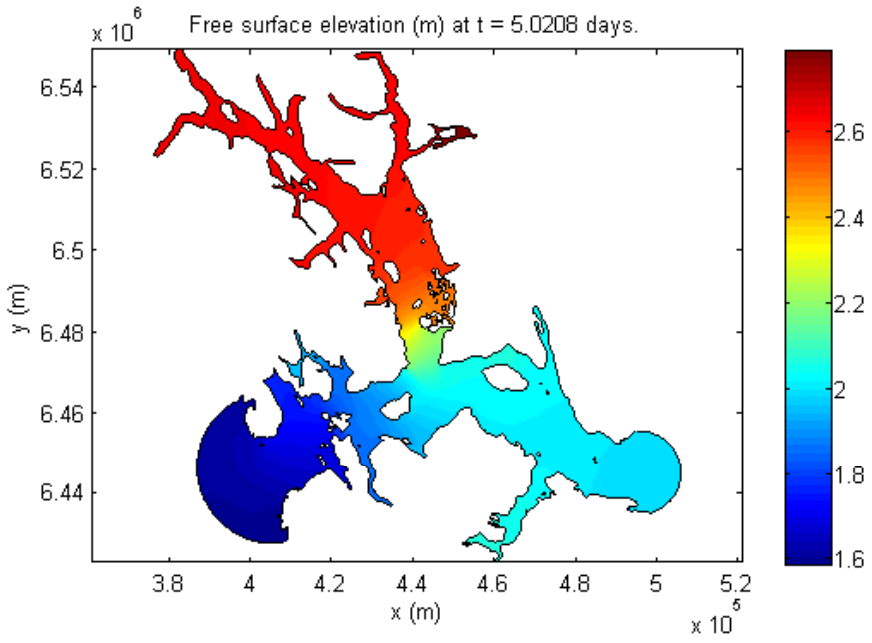

Figure 9.3: Color contours of water surface elevation.

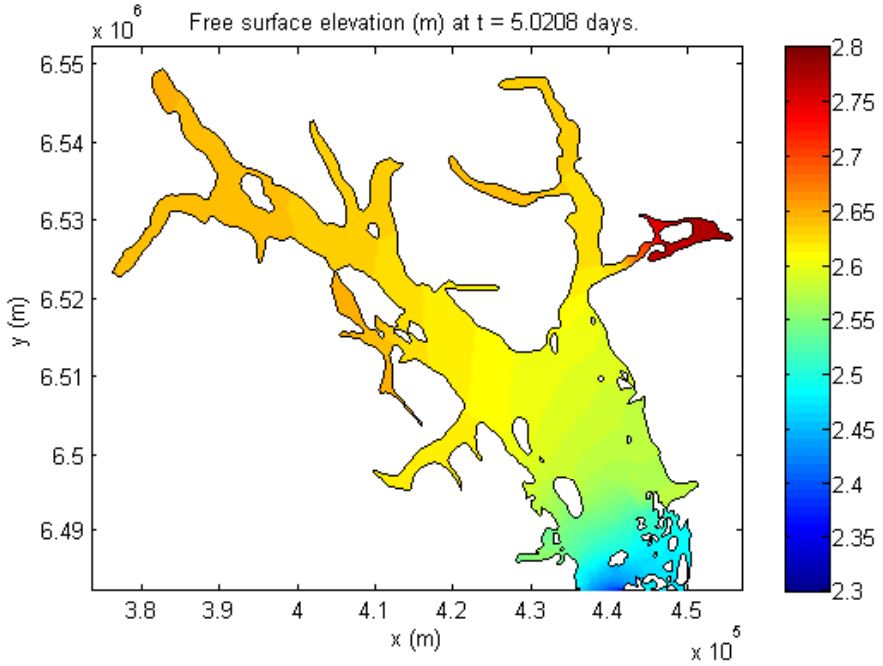

Figure 9.4: Color contours of water surface elevation in Glacier Bay proper.

9.1.2 Spatial Variation of Tidal Datums

As discussed in previous chapters, ADCIRC has the powerful ability to perform harmonic analysis of model output. This is essentially a least-squares analysis that fits model output to a user-specified number of tidal constituents. For each tidal constituent, the amplitude and phase is computed by the analysis. This information can then be used to compute tidal datums, such as mean higher high water (MHHW), mean lower low water (MLLW), and so on. These tidal datums are useful long-term indicators of the tidal conditions at a given location.

For the present application, a harmonic analysis was performed by conducting a 90 day simulation with a 20 day ramp. The last 45 days of the simulation period were used for the harmonic analysis. The results of the harmonic analysis, in terms of constituent amplitudes and phases, were then analyzed using the harmonic constant datum method (Mofjeld *et al.*, 2004). The results for MHHW, MLLW, and tidal range, here defined as the different between MHHW and MLLW, are shown in Figs. 9.5-9.7.

Note first of all the presence of numerous locations that seem discontinuous. For example, the region to the southeast of Point Gustavus. This has to do with the presence of very shallow regions that 'dry' during the simulation. The dry periods significantly affect the calculation of tidal constituents and, in turn, the tidal datums.

Second, the tidal datums show the same sort of behavior that was observed in the instantaneous 'snapshot' of the water surface (Fig. 9.3). The tides are lowest out in the Gulf, higher in Icy Strait and Cross Sound, and higher still inside Glacier Bay proper. Tidal ranges in excess of 4.5 meters are observed in most of Glacier Bay.

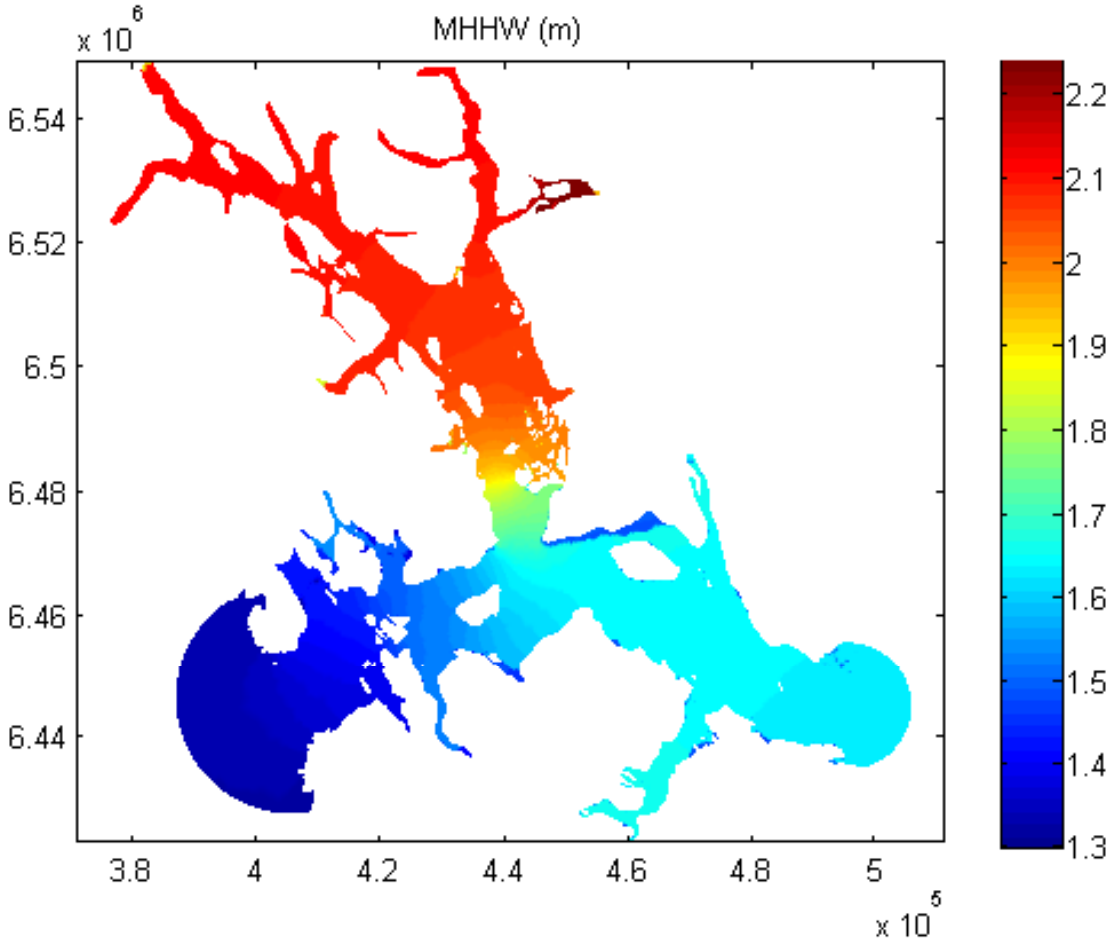

Figure 9.5: Color contours of MHHW in meters.

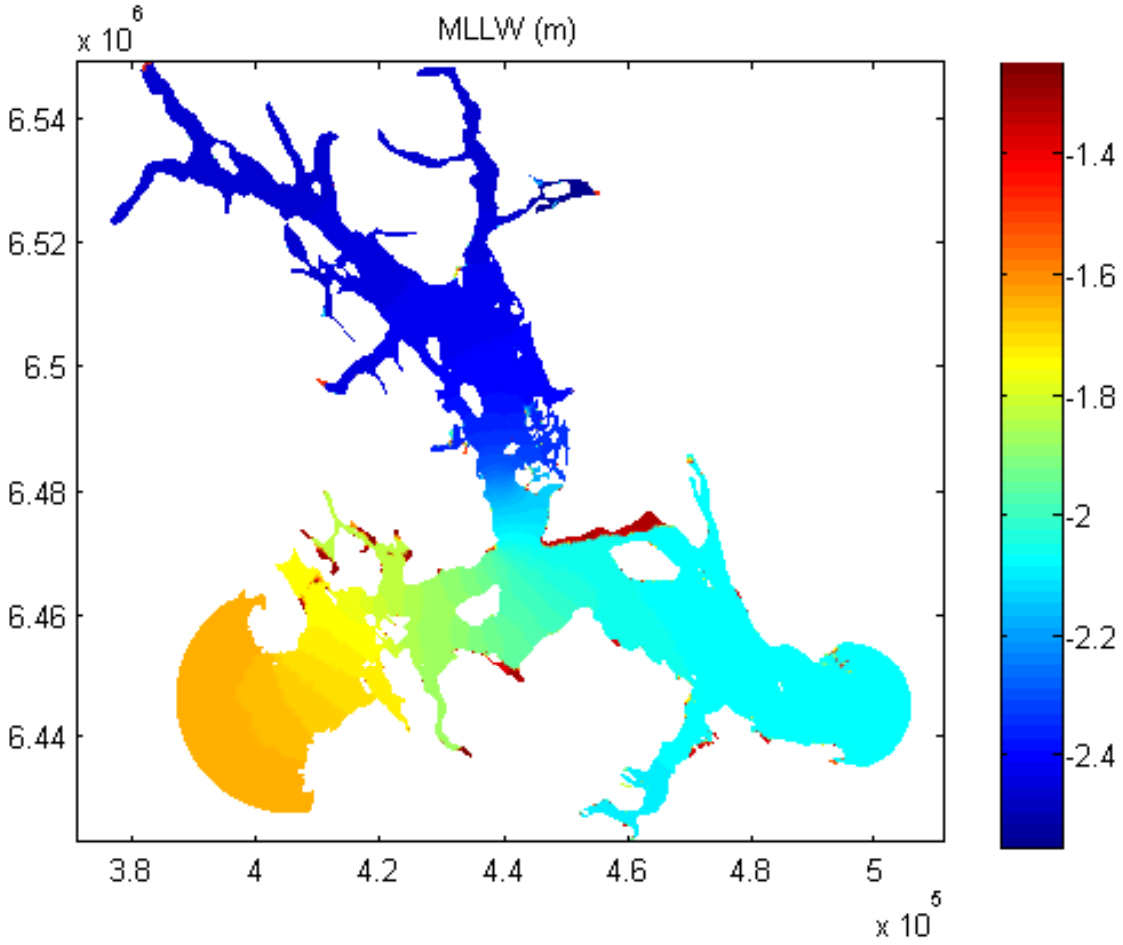

Figure 9.6: Color contours of MLLW in meters.

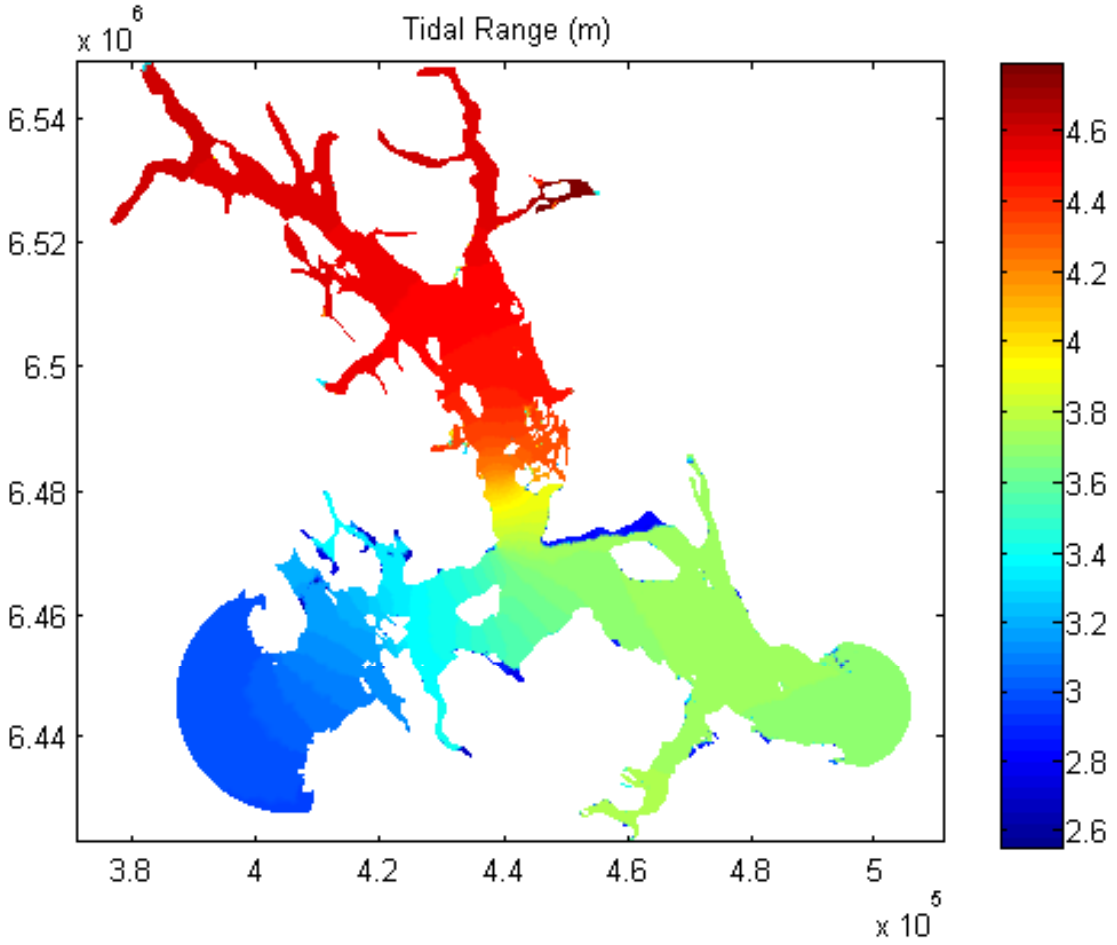

Figure 9.7: Color contours of tidal range in meters.

9.2 Tidal Velocity

The previous section demonstrated that the water surface elevation varies across the domain, but only weakly. The results for tidal velocity, in contrast, are completely different. This is due primarily to the extreme gradients in bathymetry and in channel width that exist in Glacier Bay.

An instantaneous snapshot of tidal velocity, such as given in Fig. 9.8, clearly reveals the very strong variability in tidal speed. Given that tidal speed is a good proxy for tidal mixing and vertical stratification, an understanding of the spatial variation in the velocity results is of great importance.

Additionally, many interesting features can be observed through a careful analysis of the velocity results. For example, Fig. 9.9 illustrates a very complex series of eddies that form in the Sitakaday Narrows area (between Rush Point and Young Island) when the tide changes from ebb to flood and vice versa. This computationally confirms the abundant anecdotal accounts of strong tide riffs in this area. This eddying behavior can be found at numerous other locations within the domain.

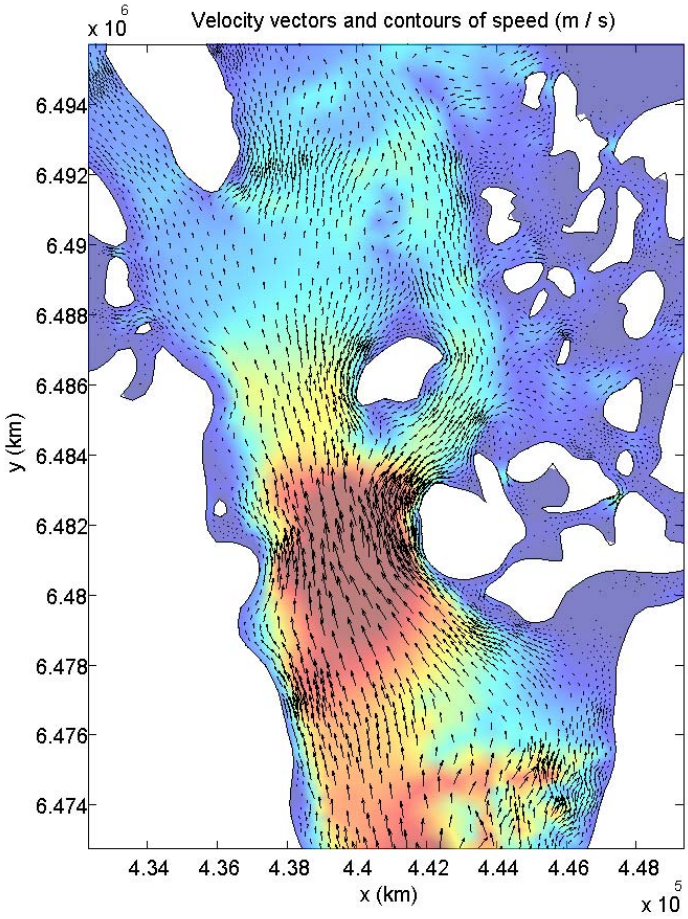

Figure 9.8: Sample velocity vectors showing the two-dimensional flow field and contours of water speed in the Sitakady Narrows area.

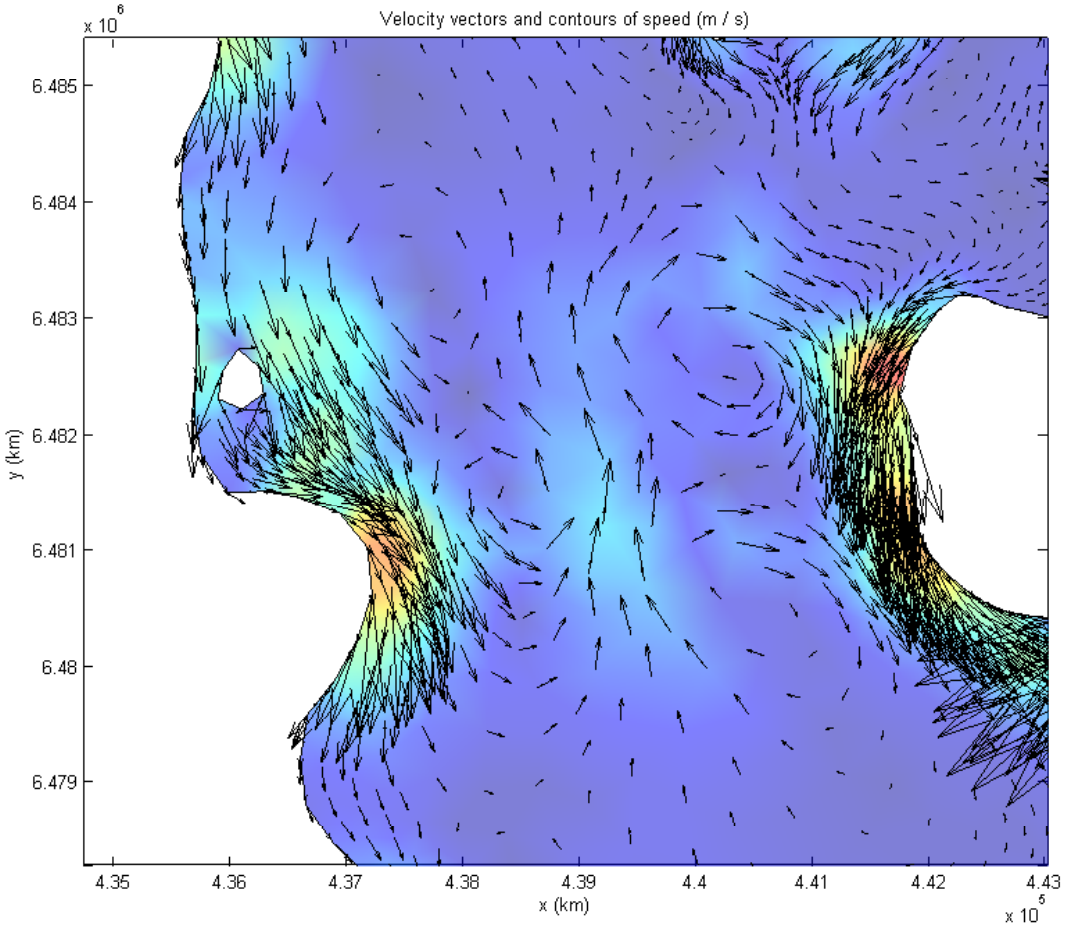

Figure 9.9: Illustration of complex eddying in Sitakaday Narrows, between Young Island and Rush Point.

9.2.1 Root Mean Square Tidal Speeds

It is perhaps most illuminating to, much as was done with the computation of tidal datums, consider some sort of long term average value for tidal velocity. To that end, it was decided to calculate the room mean square tidal speed throughout the domain. Briefly, the root mean square value of a variable $x(t)$ is given by

$$x_{\text{rms}} = \sqrt{\frac{1}{T}\int_0^T x^2\, dt}, \tag{9.1}$$

where T is some suitable averaging time. So, if velocity data (specifically the east-west (U) and the north-south (V) velocity components) were available from a current meter, it is straightforward to first calculate the tidal speed

$$q = \sqrt{U^2 + V^2} \tag{9.2}$$

and then compute the root mean square speed from the time series.

Here, the capabilities of ADCIRC can again be exploited. ADCIRC will perform harmonic analysis of the velocity results, yielding, at every point in the domain, a set of constituent amplitudes and phases for both velocity components. This means that both velocity components are easily expressed as the sum of Fourier (sinusoidal) terms

$$U(t) = a_1 \cos(\sigma_1 t + \phi_1) + a_2 \cos(\sigma_2 t + \phi_2) + \ldots \tag{9.3}$$

$$V(t) = b_1 \cos(\sigma_1 t + \psi_1) + b_2 \cos(\sigma_2 t + \psi_2) + \ldots. \tag{9.4}$$

From this, it is straightforward to show that the root mean square speed is given by

$$q_{\text{rms}} = \frac{1}{\sqrt{2}}\sqrt{\sum a_i^2 + \sum b_i^2}. \tag{9.5}$$

The root mean square speeds for the Glacier Bay domain were calculated and are presented in Fig. 9.10. Unlike the case of elevation, the results show massive variation across the domain. In particular, note the very high speeds observed in the Sitakaday Narrows area, around Point Carolus, and in Adams Inlet. A zoomed-in view of the Sitakaday area is shown in Fig. 9.11. These results all agree with anecdotal observations of tidal currents in these areas. The maximum rms speed is found to be about 1.5 m s^{-1}. Recall, of course, that this is an average of sorts and that maximum instantaneous speeds will be considerably larger than this. For example, calculations of spring tide

conditions have shown that speeds in the Sitakaday Narrows area can be in excess of 2.5 to 3 m s^{-1}.

In contrast to these high velocities, the tidal speeds in the upper reaches of Glacier Bay are found to be extremely small. This is due to the fact that, near the head of a steep sided fjord, the tidal wave is essentially a standing wave, or anti-node. At these locations, the horizontal motion asymptotically disappears and the motion becomes purely vertical.

To help quantify this, Fig. 9.12 (Etherington *et al.*, 2004) shows 24 locations where the United States Geological Survey collected oceanographic data during the period of 1993 - 2002. The root mean square tidal speeds at these stations are summarized in Table 9.1. The results show a distinct steady decrease in speed with up-fjord distance. For example, stations 5 - 12 run from (roughly) the mouth to the head of the West Arm. and the tidal speeds steadily decrease from 5 to 1 cm s^{-1}. Stations 13 - 18 run up the East Arm and show a very similar decrease in speeds.

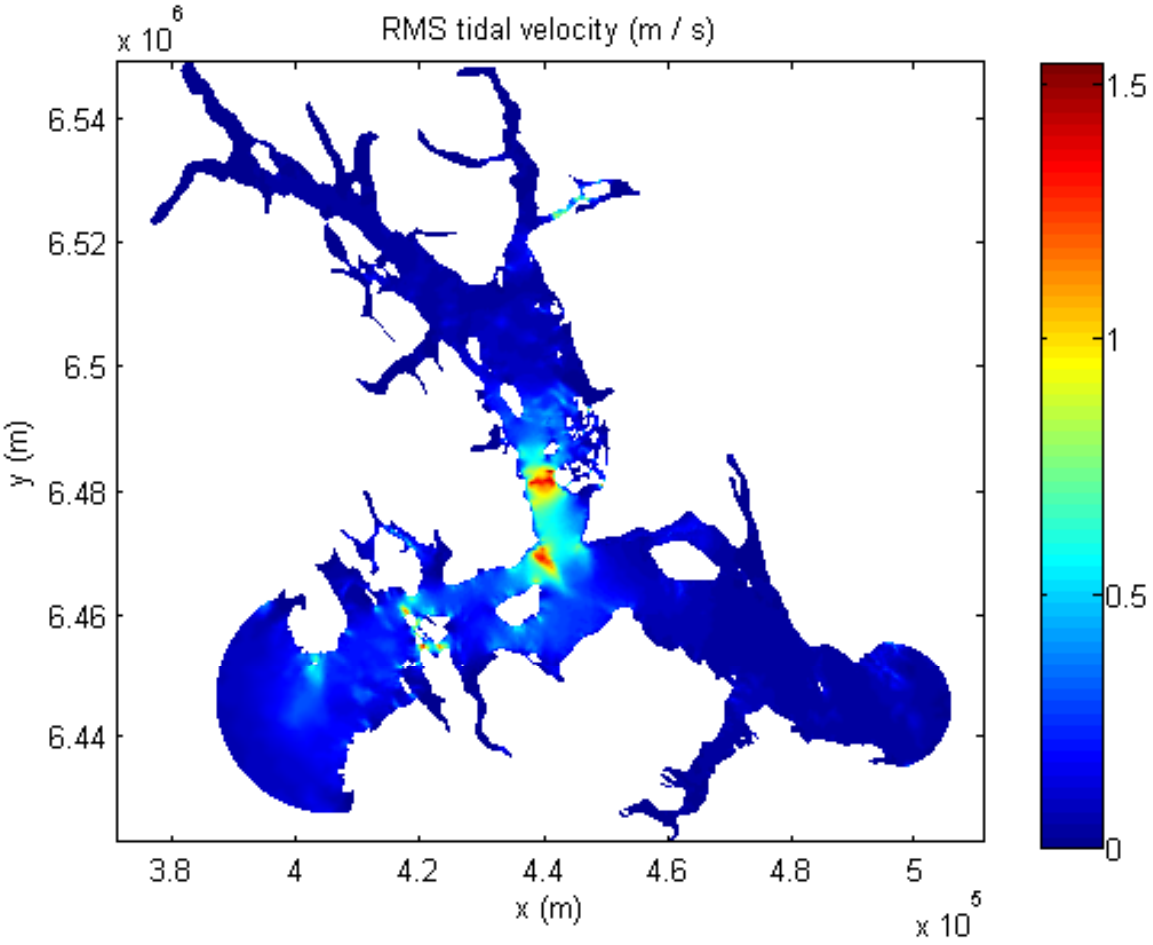

Figure 9.10: Color contours of root mean square tidal speed.

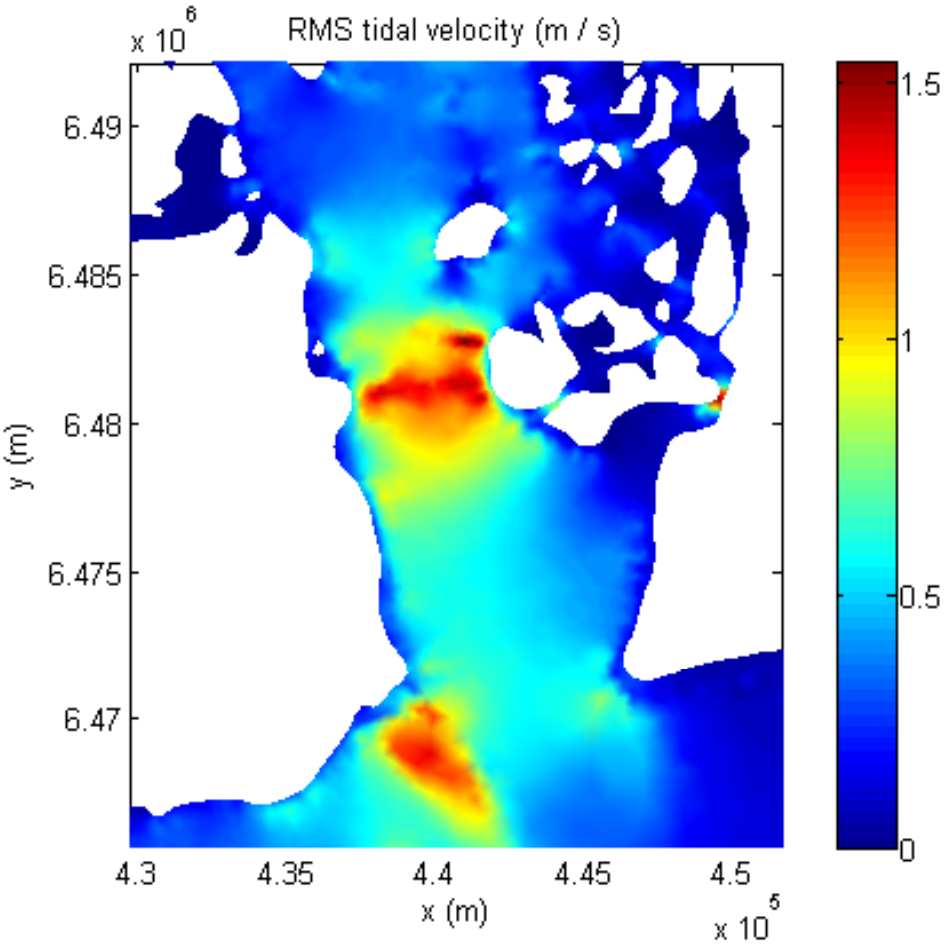

Figure 9.11: Color contours of root mean square tidal speed in the Sitakaday Narrows area.

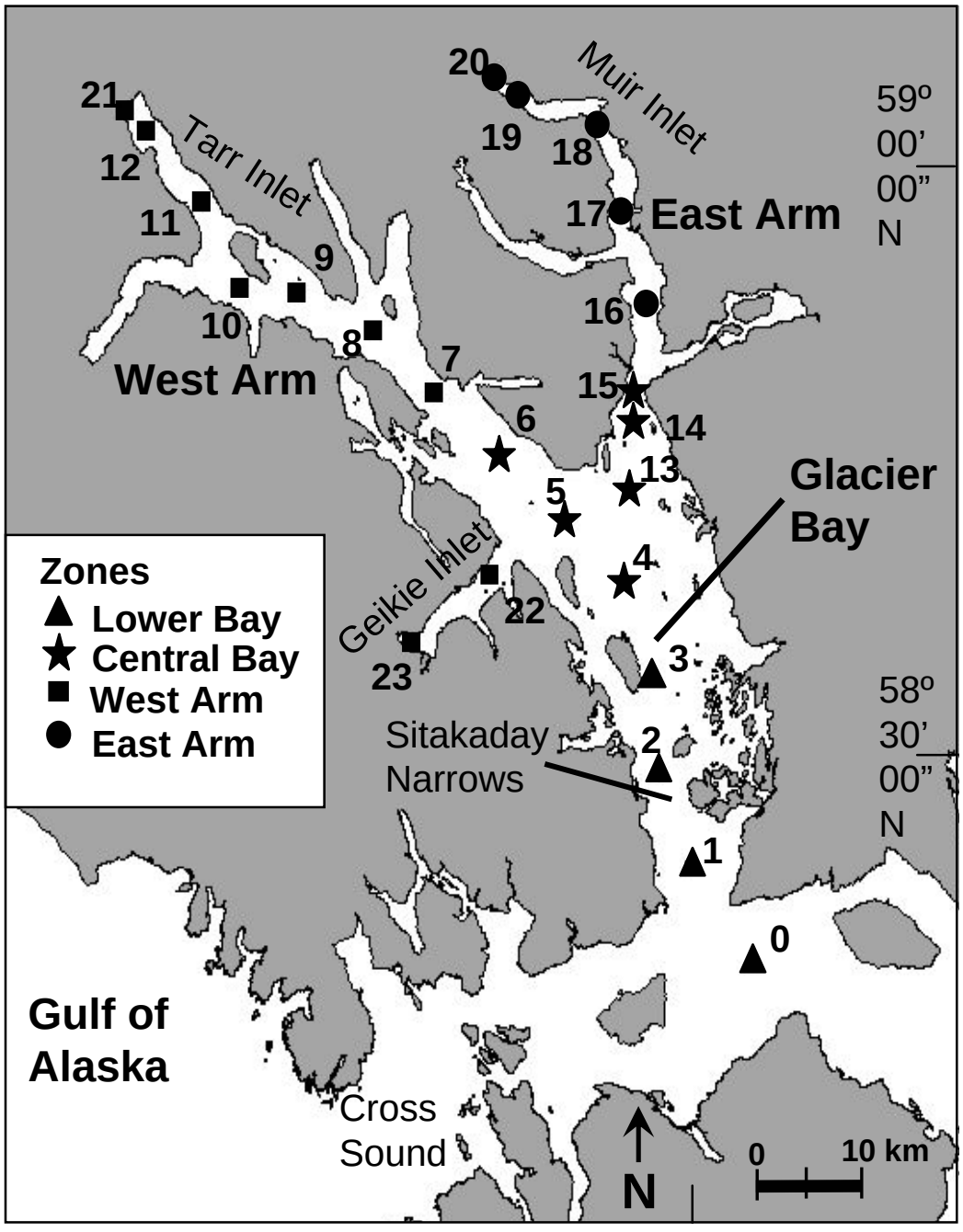

Figure 9.12: Location of oceanographic data collection stations. Figure reproduced from Etherington *et al.* (2004).

Station	RMS Speed (m s^{-1})
0	0.18
1	0.56
2	0.72
3	0.33
4	0.074
5	0.051
6	0.043
7	0.043
8	0.028
9	0.027
10	0.024
11	0.010
12	0.004
13	0.049
14	0.122
15	0.139
16	0.020
17	0.024
18	0.010
19	n/a
20	n/a
21	0.001
22	0.023
23	0.007

Table 9.1: Root mean square tidal speeds at USGS oceanographic station locations.

9.3 Particle Trajectories

The plotting of particle trajectories is an extremely helpful tool, in terms of visualizing the currents in Glacier Bay. To help illustrate this, simulations were carried out both for typical spring and typical neap tide conditions. Specifically, four trials were conducted, each reporting output for a two day period. The beginning times of these simulations (and corresponding Bartlett Cove stage) are given below:

1. March 21, 2007, 11:22 GMT, 18.2 ft H
2. March 21, 2007, 17:42 GMT, -3.5 ft L
3. March 12, 2007, 3:11 GMT, 8.7 ft H
4. March 12, 2007, 8:32 GMT, 7.1 ft L

Thus, trial 1 represents spring tides, beginning with an ebb, trial 2 spring tides beginning with a flood, trial 3 neap tides beginning with an ebb, and trial 4 nea tides beginning with a flood.

Figure 9.13 gives a quick overview of how these particle trajectories vary over the Glacier Bay domain for the case of trial 2. The red dots indicating the starting points and note that the two day simulation period corresponds to about four complete tidal cycles. It is immediately clear that vast spatial gradients in tidal excursions exist within the bay. In the upper reaches of the east and west arms, the tidal motion is quite weak. Tidal excursions (maximum distance between flood and ebb points) are found to be on the order of 0.5 to 1.5 km. In the lower bay, however, the strong tidal currents produce tidal excursions on the order of 20 km.

A closer look at the lower bay region for trial 2 is presented in Fig. 9.14. One item of great interest, in terms of the exchange of bay waters with outlying waters in Icy Strait, is that there seems to exist a near 'barrier' of sorts between eastern Icy Strait and the mouth of Glacier Bay. During the flood phase, it is observed that several particles from western Icy Strait are swept into Glacier Bay and travel significant distances up-bay. The particles in eastern Icy Strait are more or less held in place.

The results for trial 1, which begins with an ebb phase, are shown in Fig. 9.15. The phenomenon referred to above again appears. Looking specifically at the particles that start at the bay mouth, all but one are swept to the west during the initial ebb. Additionally, it is observed that most of the

particles starting at the bay mouth are carried out and do not return to the bay proper.

Moving on to neap conditions, Fig. 9.16 and Fig. 9.17 show calculated trajectories for trials 4 and 3, which begin with flood and ebb phases respectively. The clear differences in these figures, when compared to Figs. 9.14-9.15, has to do with the much shorter tidal excursions. It is found that the excursions for the neap tides are roughly half those for the spring tides. In the upper bay, neap tide excursions are on the order of 0.25 - 0.75 km and in the lower bay, they are limited to about 10 km.

Finally, the complexity of tidal flows in Glacier Bay is further illustrated in Fig. 9.18, which shows trajectories for spring tide conditions in the vicinity of the Beardslee Islands. While the figure is quite visually busy, it is clear that the fate of a particle is very strongly dependent upon its initial position. Some trajectories do not stray far from their initial positions. Others find their way into 'conveyer belts' of very high tidal velocity and are therefore able to travel very far. In particular, particles that are able to make it out of the channel between Lester and Young Islands find themselves in a region of very high velocity. Additionally particles that make it into the channel separating Young and Strawberry islands experience similarly high velocities and lengthy tidal excursions.

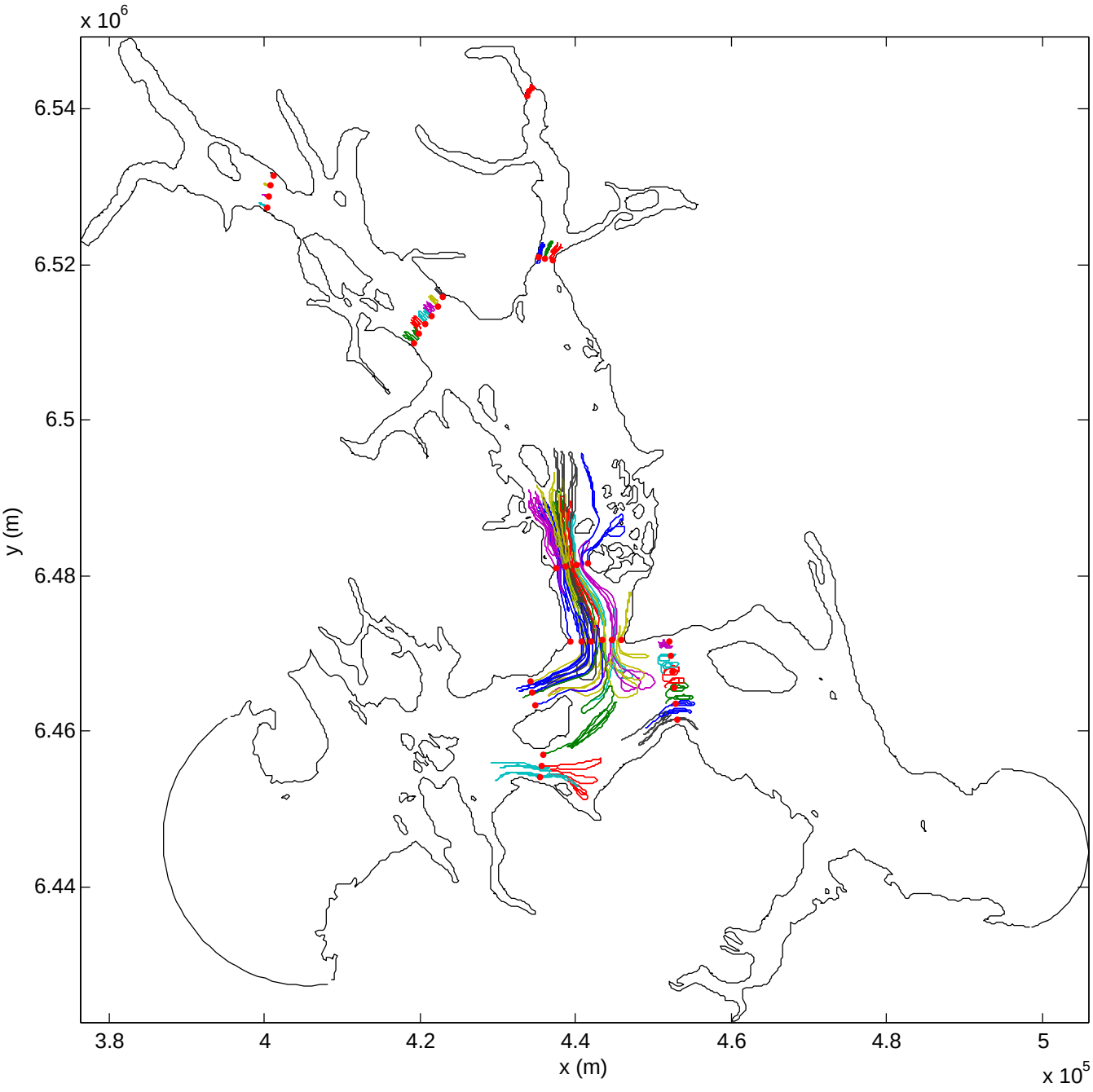

Figure 9.13: Particle trajectories for trial 2 for the entire domain.

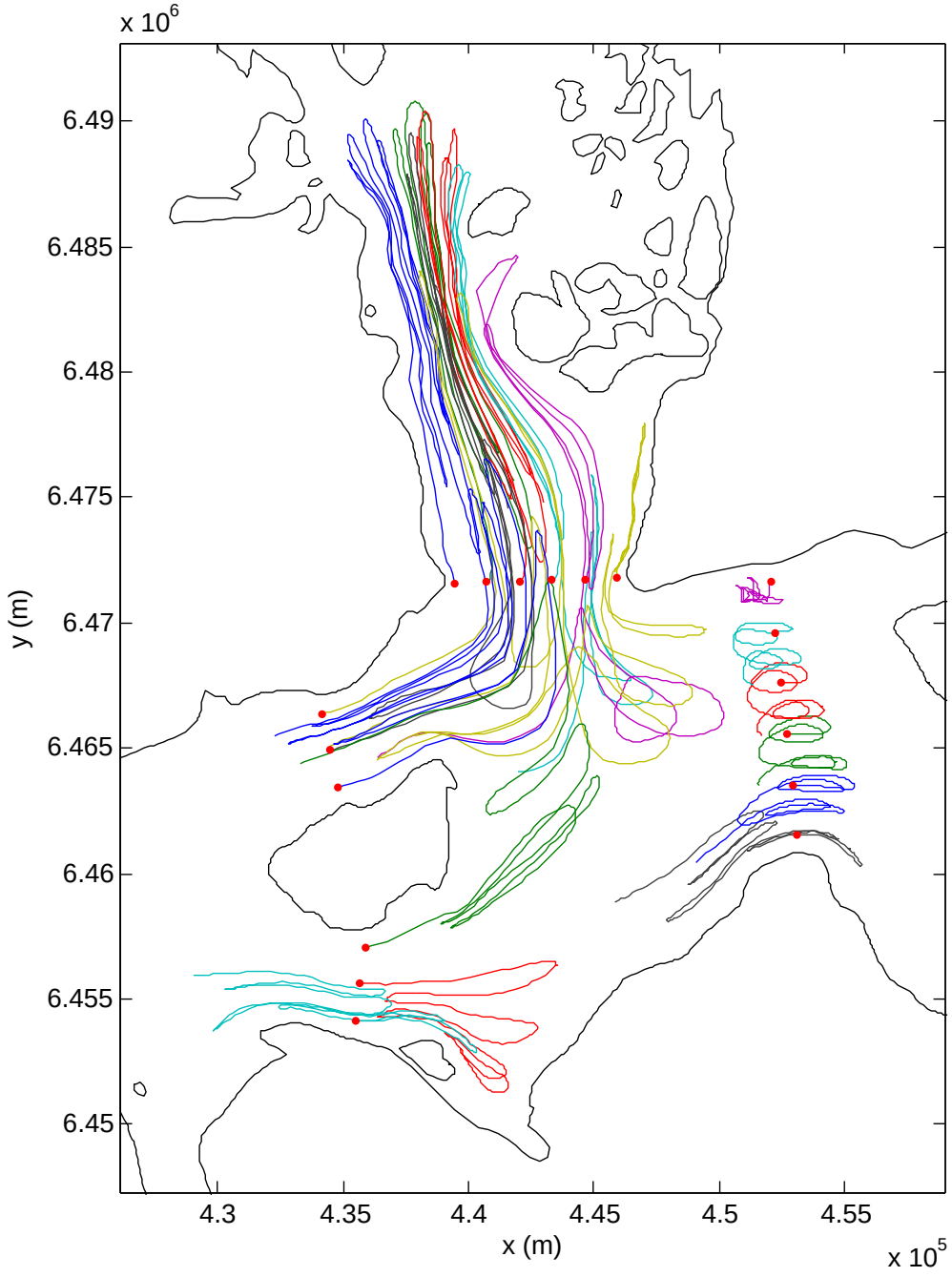

Figure 9.14: Particle trajectories for trial 2 for the lower bay region.

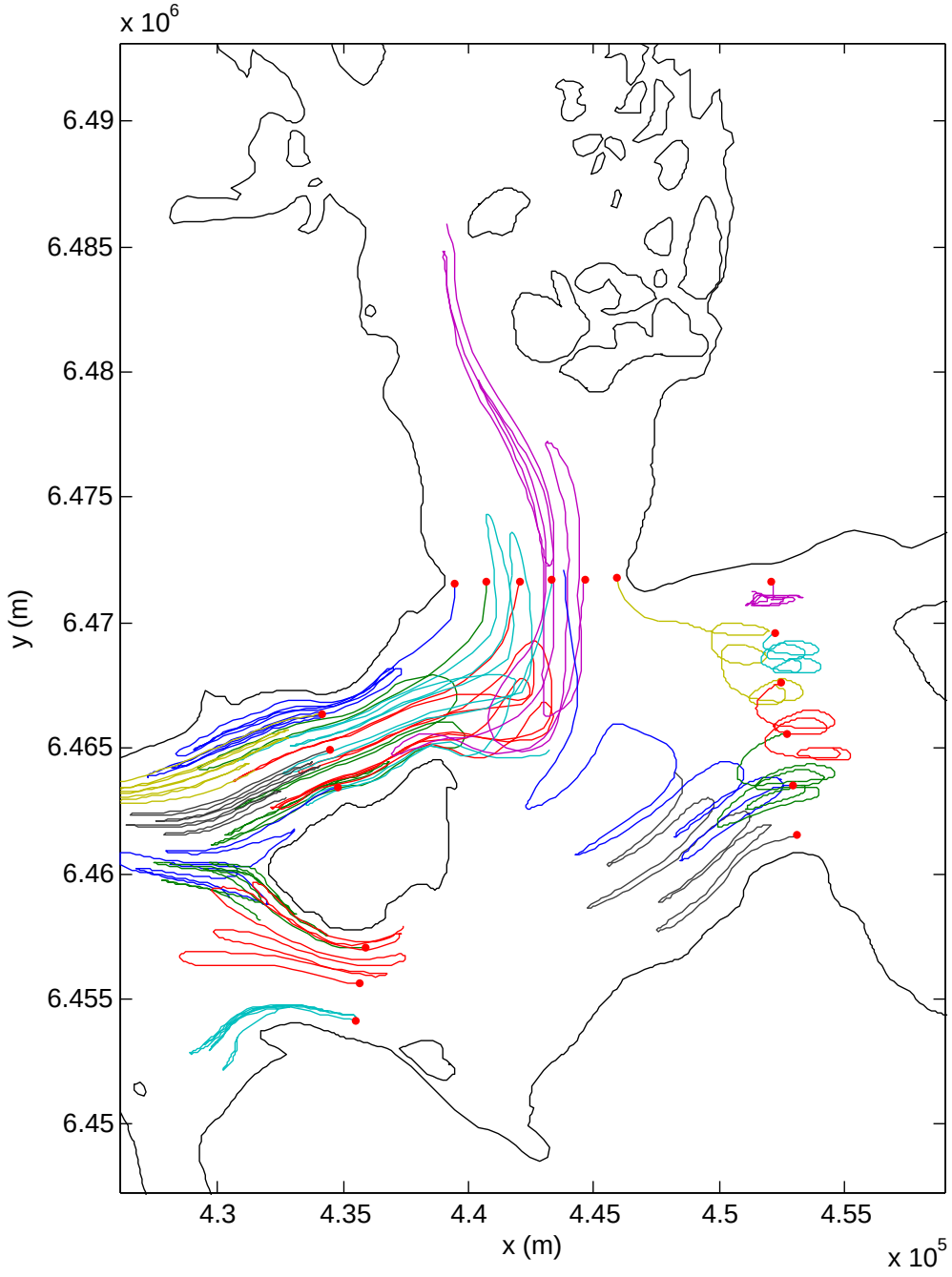

Figure 9.15: Particle trajectories for trial 1 for the lower bay region.

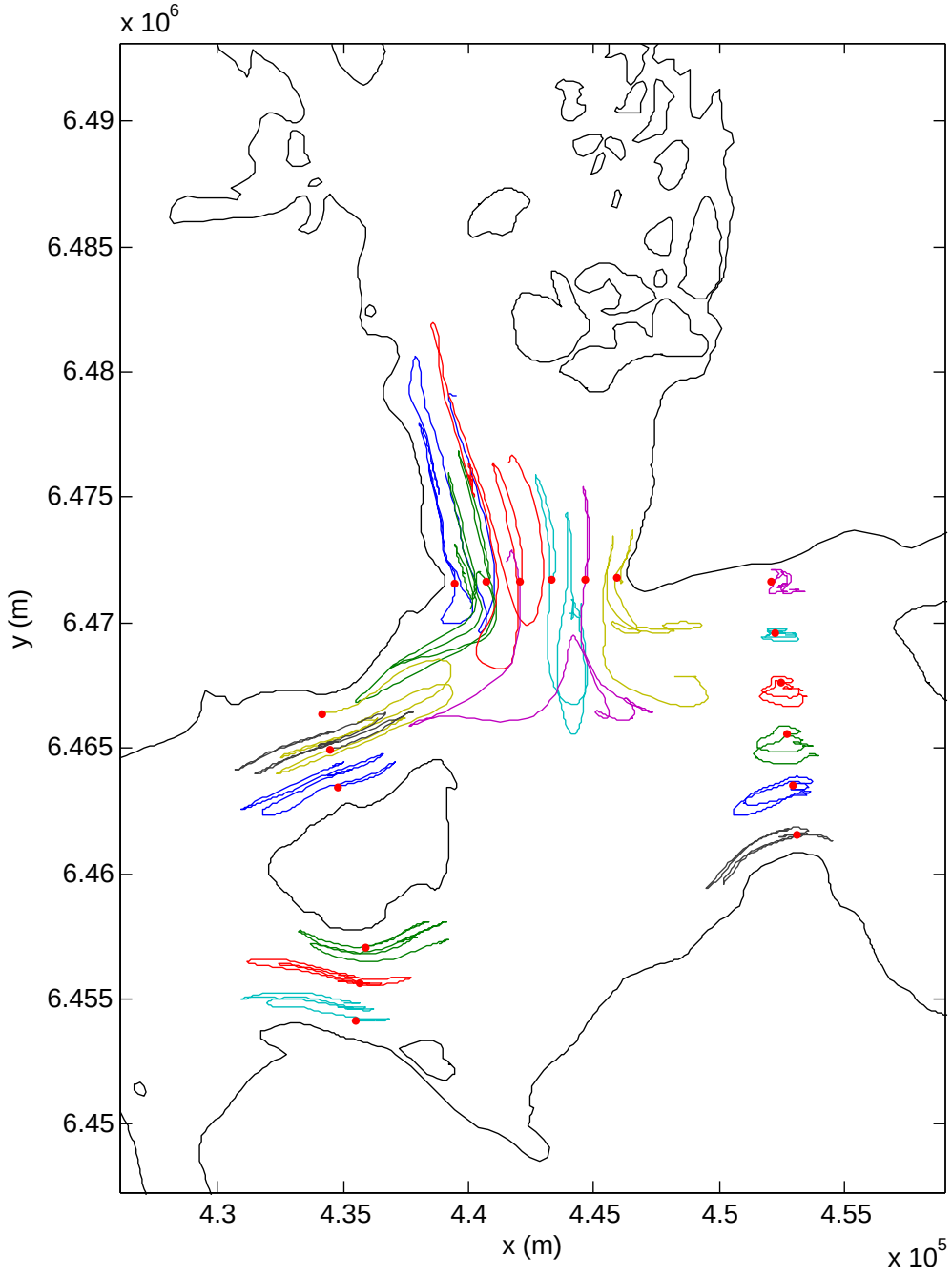

Figure 9.16: Particle trajectories for trial 4 for the lower bay region.

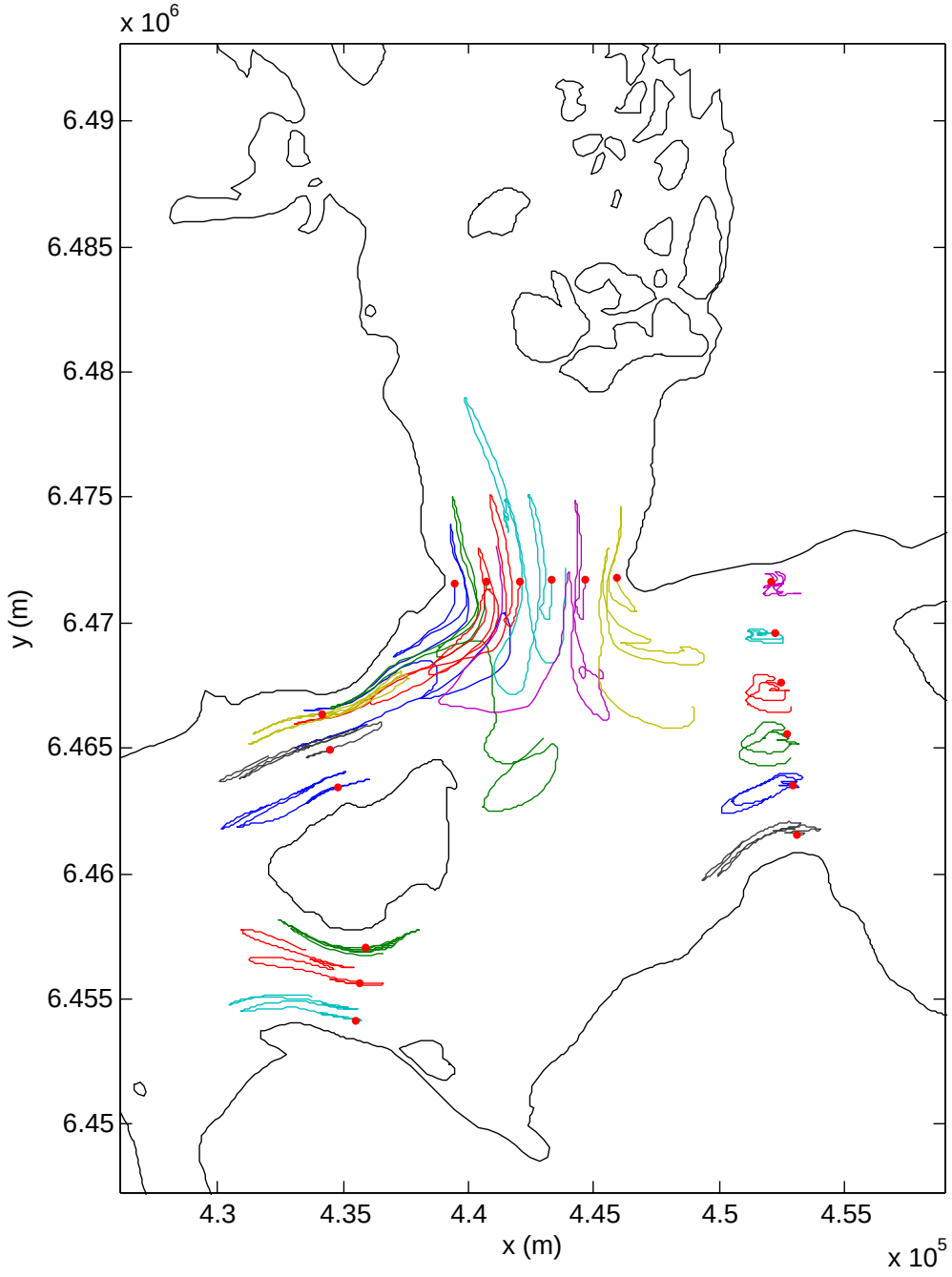

Figure 9.17: Particle trajectories for trial 3 for the lower bay region.

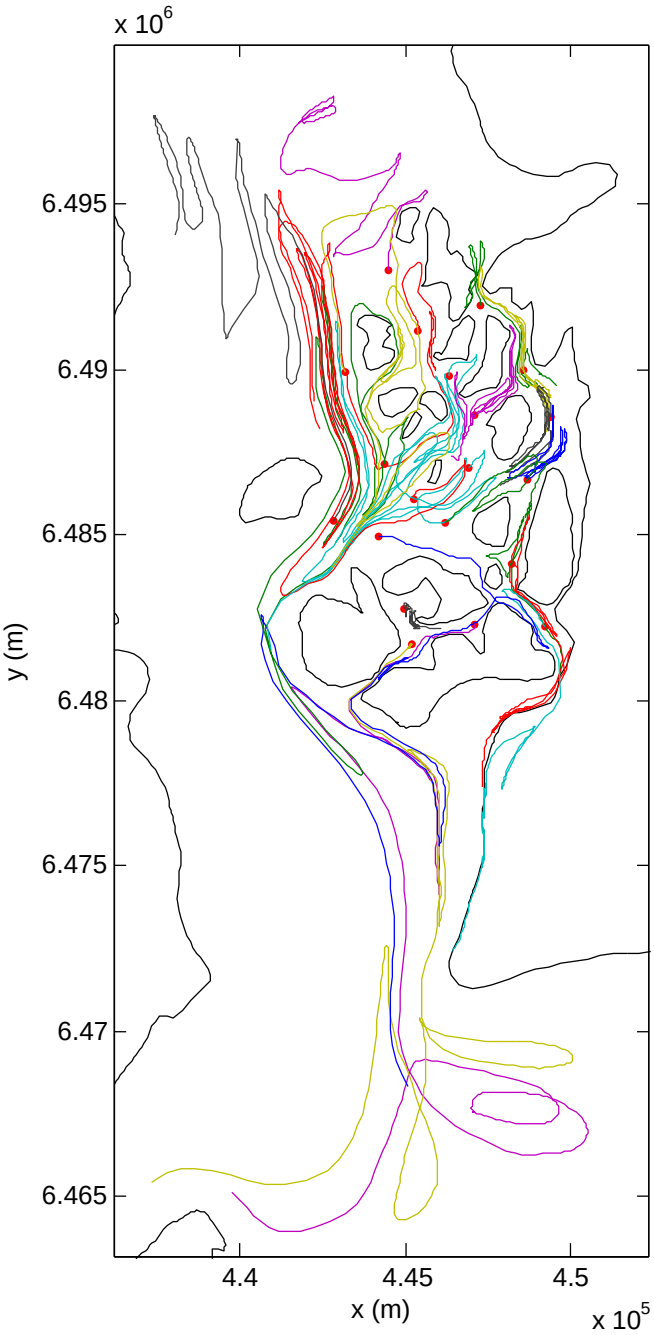

Figure 9.18: Particle trajectories for spring tides in the Beardslee Islands area.

9.4 Influence of Meteorological Forcing

As discussed in Chapter 6, a database of meteorological conditions was prepared for the Glacier Bay region. This database covers the period from 1988 to 2006 and describes hourly wind speed and direction and surface pressure. Based upon this database, fort.22 files are easily prepared by the user if a run with meteorological forcing is desired.

To test the significance of the wind, two simulations were carried out. Both lasted for 7.25 days, beginning at 17:38:51 (GMT) on 18 June, 2002. For the first simulation, meteorological forcing was suppressed while, for the second, it was included. The relevant wind data are presented in Fig. 9.19. Time series of elevation and velocity data were requested at five recording stations for the entire simulation period files. These stations are at (roughly) Elfin Cove, Bartlet Cove, Willoughby Island, Muir Inlet, and Composite Island (Fig. 9.20). Additionally, global velocity output was requested, on a five minute time step, for the last 0.25 days of the simulation period.

9.4.1 Velocity Data

Figure 9.21 summarizes the effects of the wind and pressure forcing on the x and y components of tidal velocity. Specifically, the absolute value of the difference between the 'wind' and the 'no wind' calculations is shown for each of the five locations. Note that the results are normalized by the maximum value of (no wind) tidal velocity at each of the recording stations. In this way, the data give a *relative* measure of the meteorological influence.

The results for the two velocity components are fairly similar, with a maximum difference of about 35%. This fairly large difference suggests that the wind and pressure fields are quite capable of influencing the velocity fields in Bay. If Fig. 9.21 is compared to Fig. 9.19, the observed wind speeds appear to correlate fairly well with the observed differences in the calculations. For example, the peaks in wind speed observed (roughly) at days 1, 2, 5, 6, and 8 match up with similar peaks in the difference curves. Additionally, the relatively quiet period (in the wind record) between days 2.5 and 4.5 is matched by a period of good agreement between the wind and no wind calculations.

9.4.2 Elevation Data

Figure 9.22 illustrates, in a similar fashion to the previous figure, the effect of the wind / pressure forcing on the predictions of water surface elevation. Again, the differences in the data are normalied by the maximum values of elevation recorded at each station. Unlike the velocity results, where differences of up to 35% were observed, Fig. 9.22 suggests that meteorological forcing has a negligible effect on the water surface elevation. Indeed, the maximum observed difference is less than one half of one percent. Given some consideration, this is not a surprising result. The wind stress is applied tangential to the water surface. So, while it is able to 'drag' the water column horizontally and influence the velocity field, it has only a limited ability to raise or depress the water surface. It must be noted that, for the simulation period considered here, the observed wind speeds were relatively low. More extreme wind conditions will result in increased differences between the 'wind' and 'no wind' cases.

9.4.3 Calculated Trajectories

Given that particle trajectories (see §7.3) are determined through the integration of the velocity fields, the large differences observed in Fig. 9.21 suggest that similarly large differences may be found in the trajectories. Note that this is dependent upon location; Fig. 9.21 revealed a wide range of degree of agreement, depending upon location within the bay. Also, note that the relative directions of the wind and the tides can serve to mitigate or exacerbate trajectory differences. For example, if the wind opposes the tide on flood and then changes direction to oppose the tide on ebb, the net effect on a particle trajectory may well average out to zero over the diurnal cycle. It is furthermore anticipated that trajectory differences will be cumulative in time, leading to larger and larger errors as the simulation period increases.

The two simulations described above can be used to investigate the effects of climate on particle trajectories, although they are limited (0.25 day) in duration. At $t = 7$ days, particles were released at the five stations considered above. For the next 0.25 days (running to the end of the simulation period), trajectories were compared for the 'wind' and 'no wind' cases.

Table 9.2 summarizes the total distances traveled by the particles. Note that the total distance traveled is computed by integrating along the path taken; it does *not* simply reflect the linear distance between starting and

ending points. The table also gives the distance (Δs_e) between the endpoints of the 'wind' and 'no wind' runs. Finally, this difference is normalized by the 'no wind' distance traveled in order to give a non-dimensional measure, (Δs_e^*), of the error in neglecting the wind.

For regions characterized by relatively strong tidal velocity, say locations 1 - 3, the error is fairly slight. However, in regions characterized by weak tidal velocity, locations 4 and 5, the error can be very significant. In these locations, the drift velocity induced by the wind is comparable to the tidal velocity, leading to large errors. As these results show, if the goal is to accurately predict the paths taken by material elements, the effects of even modest winds are non-negligible and should be included in the ADCIRC simulations.

Location	Total (no wind) distance (km)	Total (wind) distance (km)	Δs_e (m)	Δs_e^*
1	7.62	7.75	107	0.014
2	4.01	4.06	1	0.0003
3	1.79	1.78	121	0.067
4	0.72	0.71	283	0.39
5	0.94	1.09	269	0.29

Table 9.2: Summary of trajectory information for particles released at 5 stations within the domain.

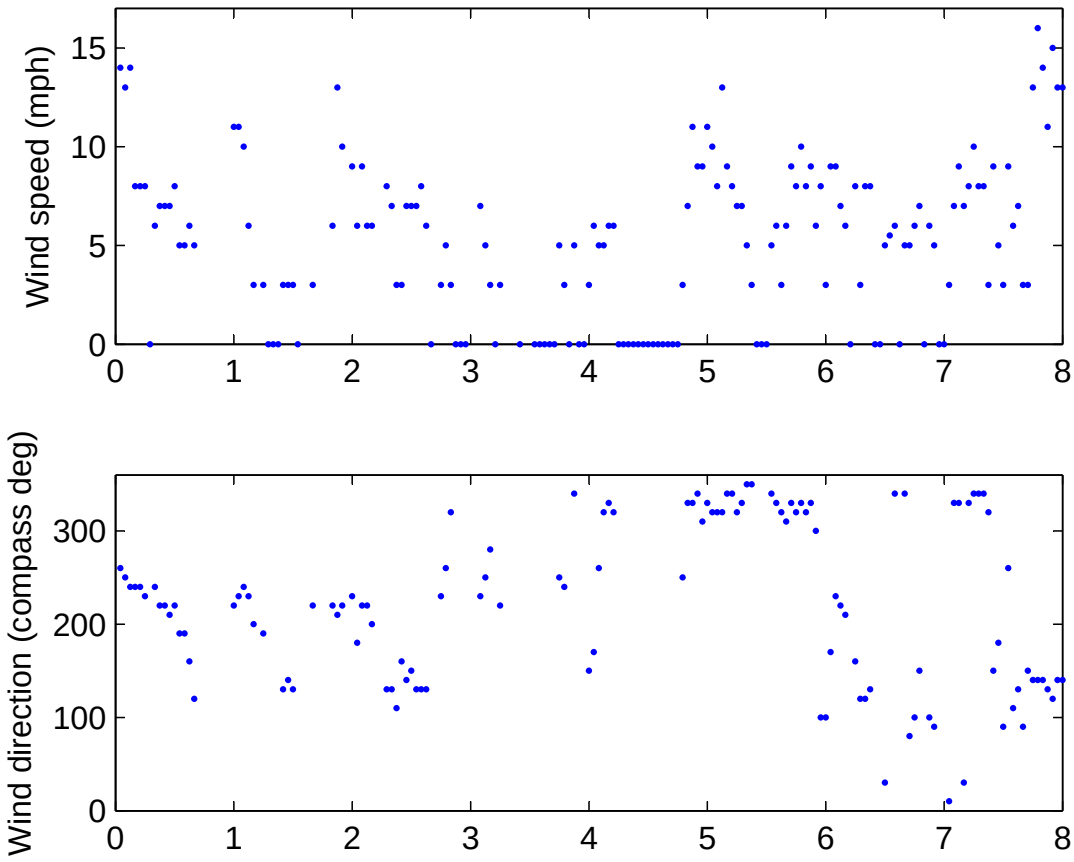

Figure 9.19: Wind speed and direction data for the period in question.

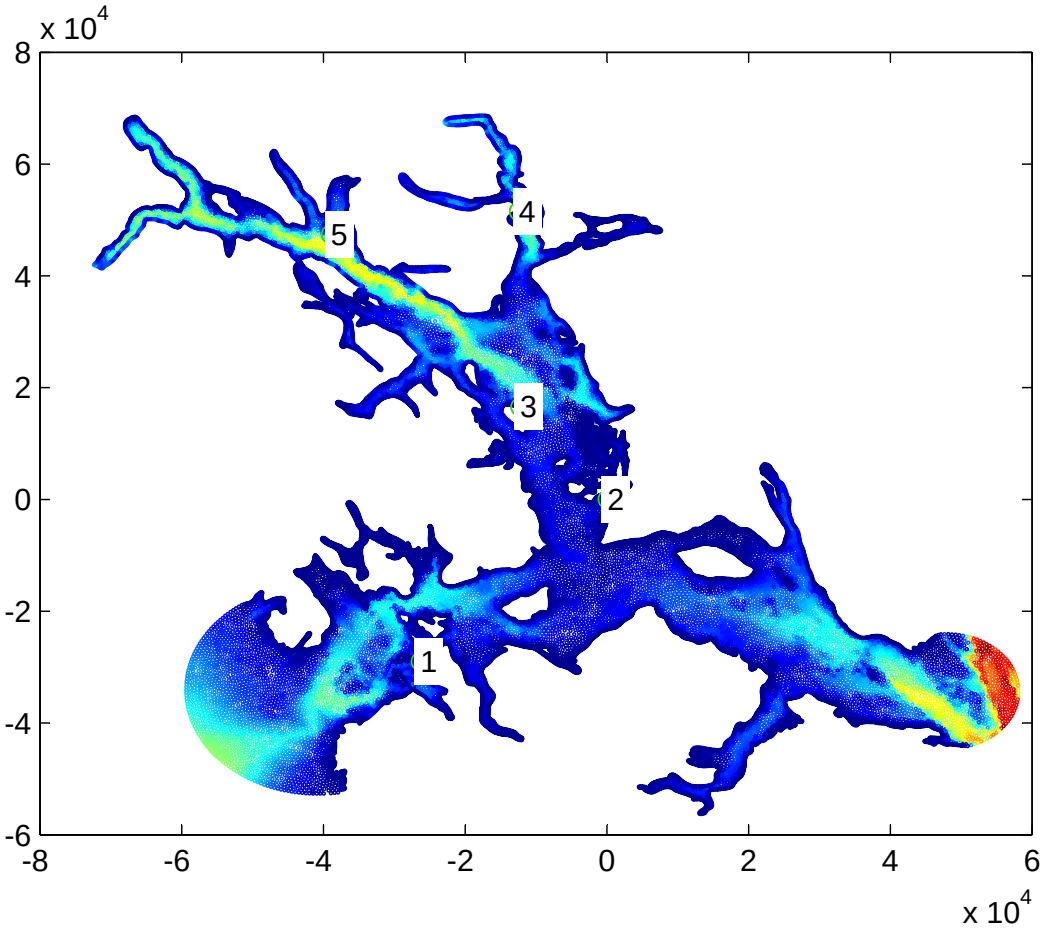

Figure 9.20: Model domain, with the five recording stations identified.

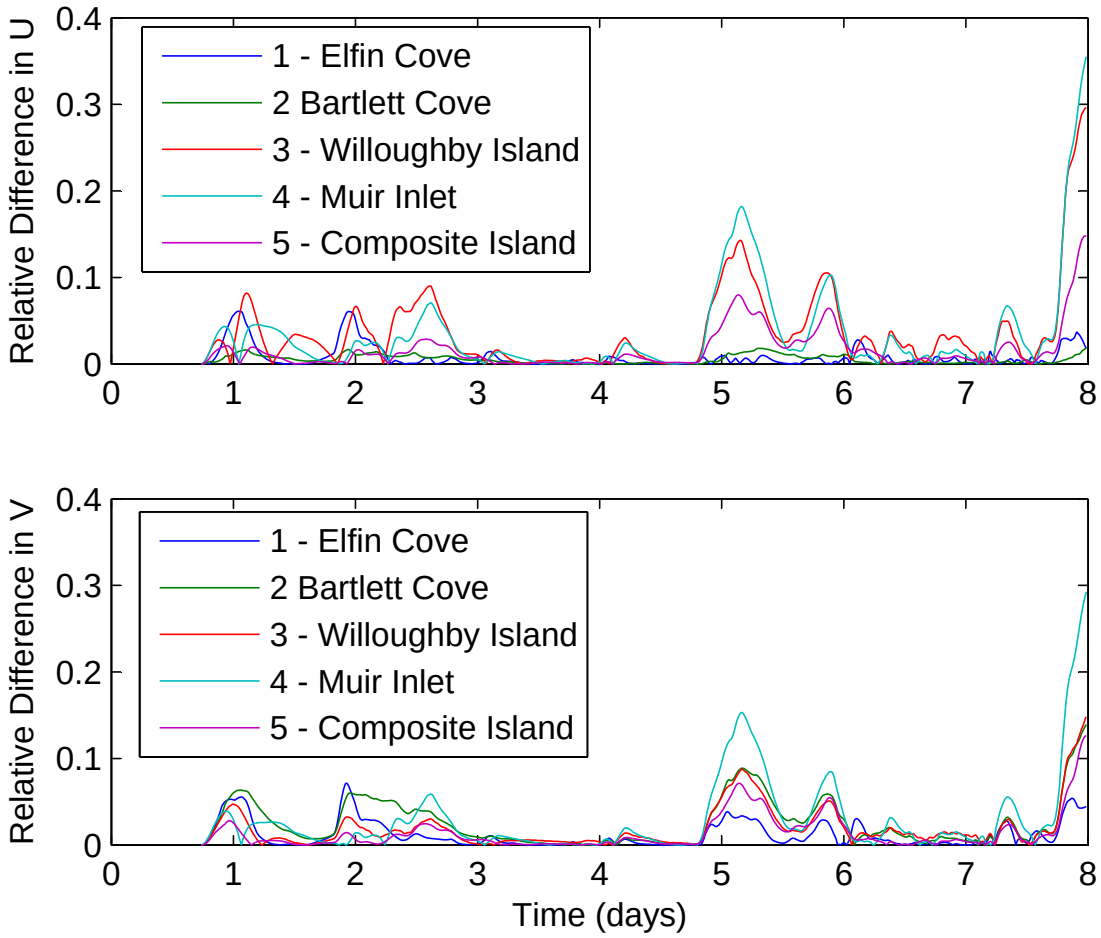

Figure 9.21: Normalized absolute value of the difference between the 'wind' and 'no wind' x and y components of velocity.

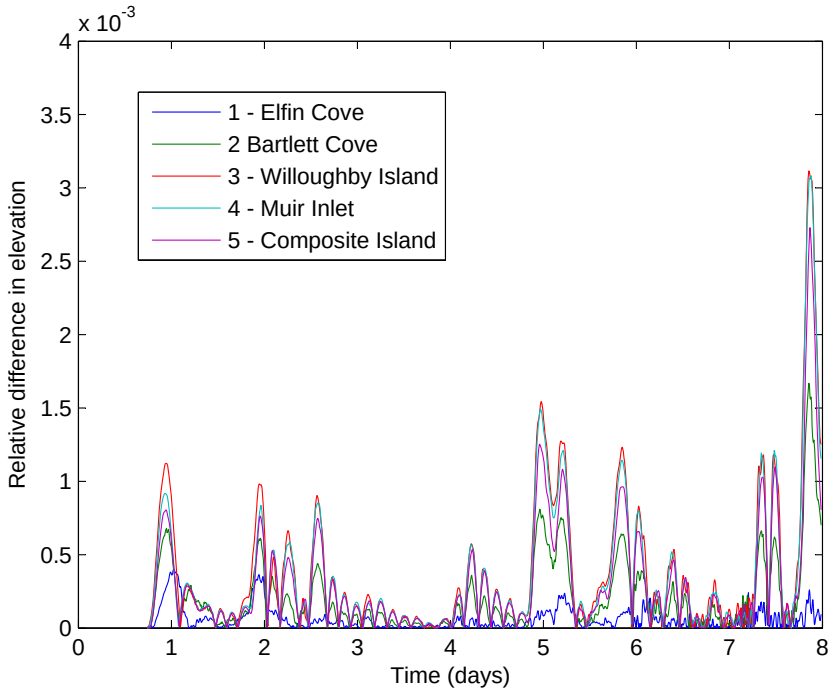

Figure 9.22: Normalized absolute value of the difference between the 'wind' and 'no wind' calculations of water surface elevation.

9.5 Influence of Inflows

Finally, it is of considerable interest to consider the significance of freshwater input to the bay. As Chapter 5 revealed, the discharges into the bay were estimated to be very considerable. These inflows will have several effects. First of all, the momentum that they impart to the bay waters will alter tidal circulation patterns. Secondly, they will result in a net seaward drift. Finally, in the context of three-dimensional modeling, the freshwater input will be a primary control on the observed vertical stratification of the water column.

As the present modeling effort is two-dimensional, the results stemming from the inclusion of freshwater inflows are of limited use. This is because, by virtue of the depth-integrated approach, the freshwater drift will be computationally distributed evenly over the entire water column. Given the large depths observed in most of the bay, this will result in quite small drift velocities. In reality, due to the stratified nature of most of the bay, the freshwater flows will be concentrated in the extreme upper layers. The net effect of this is that the present computational results substantially underpredict the expected drift. Extension of the modeling effort to three-dimensions will allow for the full utilization of the inflow estimates outlined in Chapter 5.

It *is* of value to consider the effects of freshwater inflow in the vicinity of the Sitakaday Narrows area and the bay mouth. As has been demonstrated by Etherington *et al.* (2007), this lower bay region remains unstratified to weakly-stratified throughout the year. This vigorous tidal mixing is due to the large tidal velocities in this area (Fig. 9.11) and the observed uniformity of the water column suggests that the depth-averaged approach of the ADCIRC model is adequate for handling the freshwater discharge in this area.

Figure 9.23 illustrates the influence of freshwater inputs for one simple test case. Here, a line of drifters was placed along the bay mouth at the start of a flood tide (spring conditions). The figure shows the location of the drifters at the subsequent slack water (3 hours later). The blue markers represent the absence of freshwater inputs, and the red markers represent the case where freshwater inflows (2 year peak discharge values) have been included. It is clear that the freshwater flow seaward has the effect of reducing the intrusion of the drifters into the bay.

Figure 9.24 shows the same comparison, but this time carried out for 48 hours. Here, the trajectories are shown as faint lines, for purposes of visual clarity. The key point is that, with freshwater inflows (red markers) included,

all but one of the drifters has been flushed out of the bay.

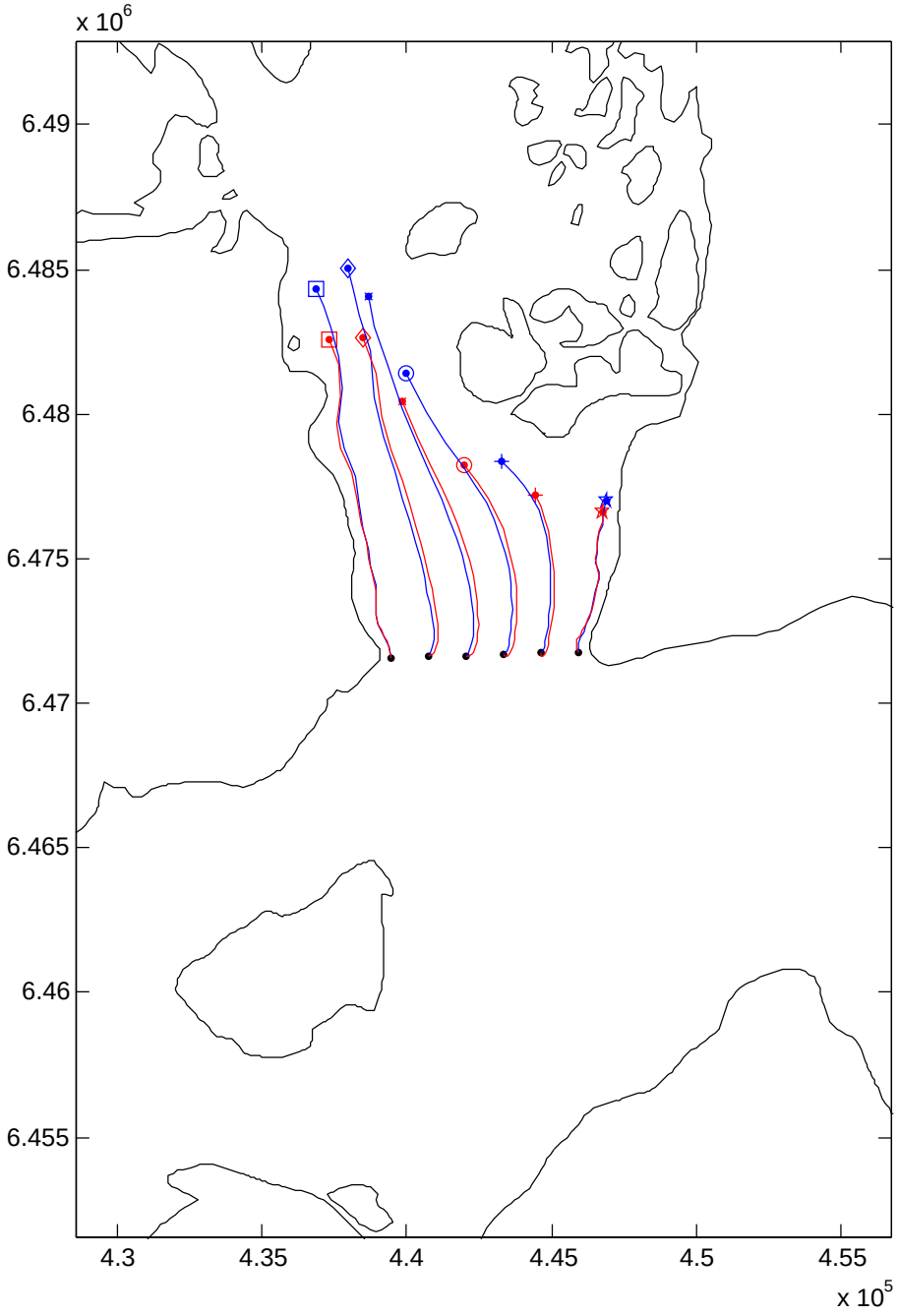

Figure 9.23: Particle trajectories, for spring tide conditions, as calculated in the presence (red markers) and absence (blue markers) of freshwater input. Tracks correspond to three hours of simulation time.

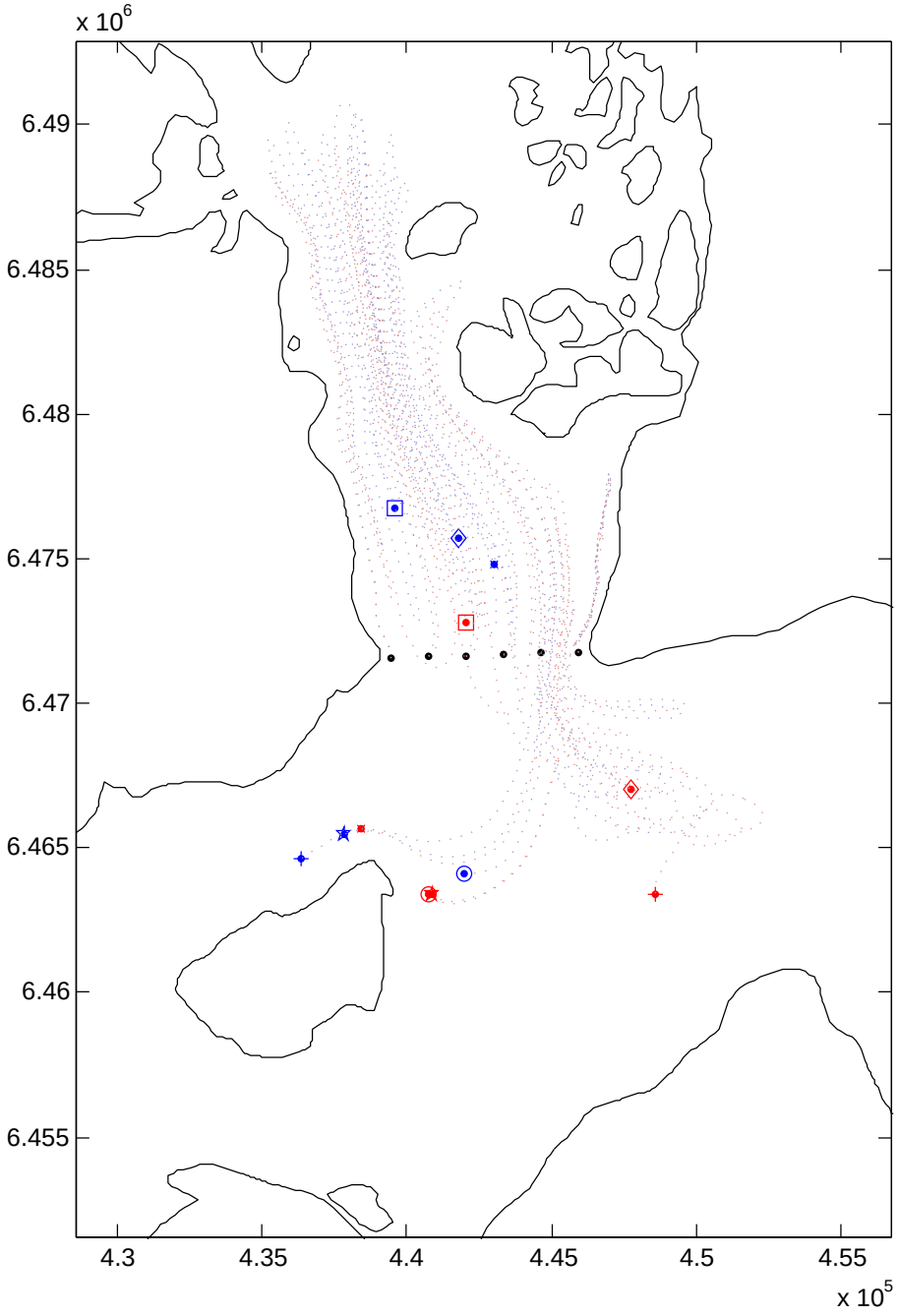

Figure 9.24: Particle trajectories, for spring tide conditions, as calculated in the presence (red markers) and absence (blue markers) of freshwater input. Tracks correspond to two days of simulation time.